Finite Element Modeling of a Microhotplate for Microfluidic Applications

Ronald P. Manginell*, David A. Rosato**, David A. Benson*, Gregory C. Frye-Mason*

* Sandia National Laboratories
P.O. Box 5800, Albuquerque, NM 87185-1425, rpmangi@sandia.gov
** Harvard Thermal, Inc., Harvard, MA, USA, Dave@HarvardThermal.com

ABSTRACT

A hand-held chemical laboratory (μChemLab) is being developed that utilizes a silicon- nitride-supported microhotplate in the front-end, gas sampling and preconcentration stage. Device constraints include low-power (<200mW at 5V), rapid heating (<20msec), and a relatively uniform temperature distribution throughout the heated area (~3mm^2). To optimize for these criteria, the electro-thermal behavior of the microhotplate was modeled using Thermal Analysis System (TAS). Predicted steady-state and transient behavior agree well with infrared (IR) microscope data and measured transient response for a low-stress silicon nitride thermal conductivity of $k_n = 6.4 \cdot 10^{-2}$ W·(cm·°C)$^{-1}$ and a convection coefficient of $h_{cv} = 3.5 \cdot 10^{-3}$ W·(cm^2·°C)$^{-1}$. The magnitude of h_{cv} is framed in the context of vacuum measurements and empirical data. Details and limitations of the IR measurement are discussed. Finally, the efficacy of methods for reducing thermal gradients in the microhotplate's active area is presented.

Keywords: Microhotplate, preconcentrator, IR microscope, chemical analysis, TAS

INTRODUCTION

An autonomous, portable, hand-held chemical laboratory (μChemLab) is being developed for the detection of selected target analytes, such as chemical warfare (CW) agents and explosives in environments that may contain more than 1000-fold higher concentrations of interferents. Thus, rapid, sensitive (1-10 ppb) and selective response, using small, low-power components is crucial, and to this end, all critical components are microfabricated. Sensitivity and selectivity are enhanced via parallel analysis channels; each gas analysis channel contains a microhotplate-based sample collector/preconcentrator, a gas chromatographic (GC) separator, and a chemically selective surface acoustic wave (SAW) array detector [1].

The microhotplate-based preconcentrator (Figure 1) is required, based on system-level restrictions, to operate with less than 200 mW at 5V in the steady state. After selectively concentrating the desired analyte in a coating deposited on its surface, the microhotplate must attain 200 °C in less than 20 msec to thermally desorb the analyte in a pulse of temporal width sufficiently narrow for GC separation. To effect ample collection/desorption, the microhotplate must, furthermore, have a large, uniformly heated active area.

The coupled electro-thermal response of the microhotplate was simulated using Thermal Analysis System (TAS), an affordable, Windows-based thermal analysis package. Though sometimes neglected in modeling of microsystems [2], natural convection was found to be an important heat loss mechanism for this device, accounting for nearly 25% of the total heat lost. Moreover, a silicon nitride thermal conductivity, k_n, roughly twice published values [3] was required. Explanations for the magnitudes of k_n and h_{cv} will be offered. Because IR microscopy is important to the thermal analysis of microsystems, the details and limitations of this technique will be discussed.

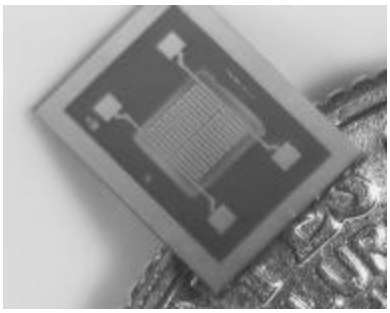

Figure 1: The microhotplate (on the edge of a quarter). "Bosch etching", stopping on the SiN membrane, was used to produce the free-standing structure.

IR MICROSCOPY

Steady-state measurements of microhotplate temperature distribution were used for model validation, and to tune the relatively unknown values of k_n and h_{cv}. A Barnes Infrascope™ was utilized for these measurements. This system employs a liquid-nitrogen-cooled array of 5 x 5 μm InSb pixels with spectral sensitivity from 1.5- 5.5 μm. Radiative emission from the sample is focused on the array by a system of IR optics. Objective lenses up to 10x are available; for the data presented here, a 5x lens with a specified spatial resolution of 8 μm and a depth of field (DOF) of 25 μm was applied.

The microscope obtains the temperature distribution, $T(x,y)$, of a sample by measuring its self-emitted radiance, $R(x,y)$, and correcting for the emissivity, ε, of the surface. A global value of ε would be quite useless for a microhotplate, given the variety of materials present. Instead, this system makes use of a two-temperature radiance technique to

Pt) is effectively opaque. For λ = 1.5–5.5 μm, $k \approx$ 7–20 [4], and transmission is 0.06–0.3%. The measured emissivity of platinum, ε_{Pt} = 0.1 agrees with published values [7]. For the reasons presented here, only measurements of $T(x,y)$ on the heater and on the die frame far from the membrane edge are suitable for comparison with model results. One final note: variations in emissivity with temperature outside the calibration range are not accounted for in this technique. With silicon, for example, this can be a deadly omission. But for platinum the effect was negligible. Temperature corrections based on emissivity variations can be estimated based on Wein's law [8].

TAS MODELING

The thermal computer modeling software, Thermal Analysis System (TAS), was employed for analysis of the microhotplate. Heat gains are attributable to Joule heating of the composite heater. Loss mechanisms modeled include conduction through the silicon nitride, the heater lines and the silicon substrate, as well as natural convection and radiation from the top surface to the ambient. Conduction in the air cavity beneath the membrane, and radiation from the backside of the membrane to the stage were also modeled. Initially, brick elements were used to represent the heater and the membrane; however, gradients through the thickness of these materials were found to be insignificant. Thus, bricks were replaced by plates to accelerate the transient solution. Both plates and bricks account for conduction in all directions, as well as add thermal capacitance to the model.

The modeling process can be summarized as follows: (a) Construction of the three-dimensional representation of the system (Figure 4). (b) Substitution of the heater's room-temperature *electrical* conductivity, σ, for a material *thermal* conductivity in TAS. (c) Application of the drive voltage, V, across the heater. (d) Solution of the model for node temperatures (voltages). (e) Conversion of the voltage distribution into elemental heat loads based on elemental voltages and electrical resistance. (f) Creation of temperature-dependent heat loads via the experimentally measured temperature coefficient of resistance (TCR) of the heater. (g) Definition of the thermal properties and boundary conditions. Unless noted, material properties were temperature independent; however, temperature dependencies may be easily incorporated. (h) Solution for the steady-state temperature and transient response.

Steady-state response

For the sake of comparison with the IR microscope data given above, the specific case of V = 4.48 V and T_s = 80 °C (i.e., the backside of the die fixed at 80 °C) was first modeled. Ambient air temperature was taken as 25 °C. Experimentally measured parameters include ε_{Pt} = 0.1, σ =

$3.66 \cdot 10^4$ $(\Omega \cdot cm)^{-1}$, and TCR = $2.4 \cdot 10^{-3}$/°C. Other relevant material thermal properties, with the exception of k_n, were borrowed from references [3,7,9].

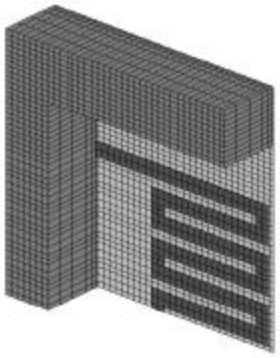

Figure 4: 3-D TAS model of a microhotplate, viewed from the etched side of the wafer (etch depth is 400 μm). By symmetry, only one quarter of the device is modeled. The heater actually resides on the other side of the membrane, but is emphasized here for illustration reasons.

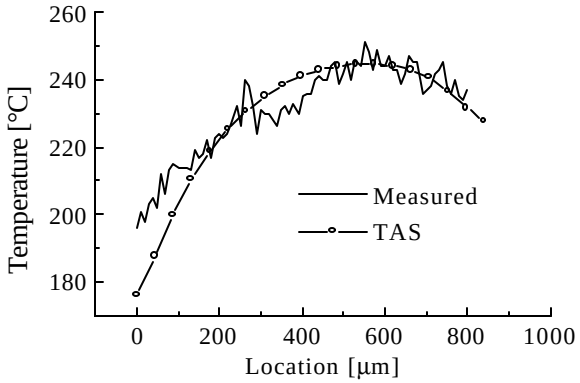

Figure 5: Temperature along the center-most heater segment. Simulation parameters are k_n = $6.4 \cdot 10^{-2}$ $W \cdot (cm \cdot °C)^{-1}$, h_{cv} = $3.5 \cdot 10^{-3}$ $W \cdot (cm^2 \cdot °C)^{-1}$ and V = 4.48 V.

At the outset, h_{cv} and k_n were relatively unknown. These parameters were adjusted to achieve agreement between simulation and experiment. First, h_{cv} was varied until the maximum heater temperature was in close agreement with the test results; h_{cv} = $3.5 \cdot 10^{-3}$ $W \cdot (cm^2 \cdot °C)^{-1}$ was required. Then, k_n was adjusted until the correct thermal gradient along the center-most heater line was attained. Initially, k_n = $3.2 \cdot 10^{-2}$ $W \cdot (cm \cdot °C)^{-1}$ was input based on reference [3]. Better agreement resulted from k_n = $6.4 \cdot 10^{-2}$ $W \cdot (cm \cdot °C)^{-1}$ (Figure 5). Figure 6 shows the simulated microhotplate temperature as viewed from its topside. Conduction to the right along the heater lead is apparent.

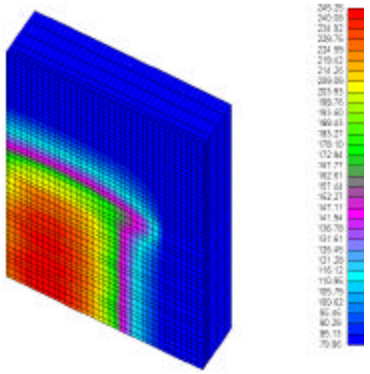

Figure 6: $T(x,y)$ with T_s = 80°C, 25°C ambient and V = 4.48 V. The scale is roughly 80 to 245 °C in 5 °C increments. (The heater's center is at the lower left corner.)

Transient response

Tests were conducted to measure the temperature response of the microhotplate. The voltage drop across a 10.6-ohm current-viewing resistor (CVR) was recorded with a digital oscilloscope after switching 4.714 V across the series connection of the microhotplate and the CVR. Using this data, the average resistance of the microhotplate was calculated. From the experimentally measured TCR of the microhotplate, the average temperature was determined. The TAS model was run for 40 msec and the average Ti/Pt temperature determined. A comparison of data is shown in Figure 7. The microhotplate reaches 90% of its set-point in t_{90} = 16 msec, and consumes 110 mW in the steady state. These values are well within design goals. Still, improvements will be sought out using the TAS model.

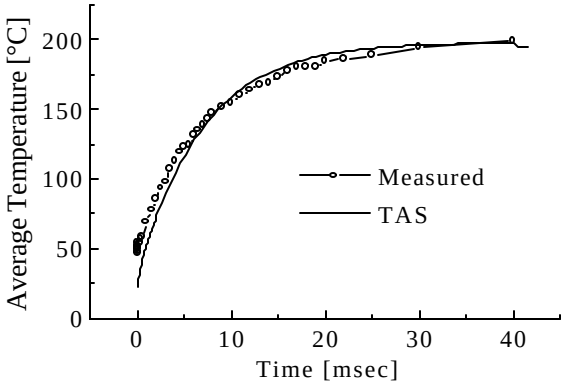

Figure 7: Comparison of the measured and simulated transient response of the microhotplate.

Temperature uniformity

Figure 8 (top) shows the temperature distribution over the heater. A gradient of more than 80°C is evident. To improve uniformity, 0.5μm of aluminum was added to the heater area (Figure 8, bottom) based on reference [2]; the

predicted gradient was reduced to 14°C without significantly impacting the system's time response.

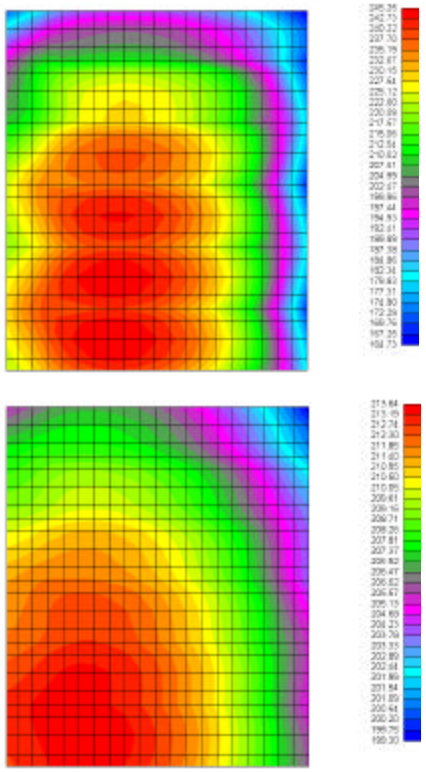

Figure 8: $T(x,y)$ in the heated area for the existing design (top) and with 0.5 μm of Al added (bottom). Top scale: 164.73-245.25°C by 2.5°C. Bottom scale: 199.03–213.64°C by 0.45°C. (The heater's center is at the lower left.)

Discussion

Natural convection coefficients obtained empirically from large flat plates typically range from $7{\cdot}10^{-4}$- $2.8{\cdot}10^{-3}$ $W{\cdot}(cm^2{\cdot}°C)^{-1}$ [10]. In this regime, edge effects can usually be ignored. This is not necessarily true of microsystems where heated areas are comparatively small, and convection coefficients larger than bulk values may be expected in this regime. Power consumption of a square microhotplate, 0.8 mm on a side, was measured at 630 Torr and 70 Torr for an average ambient/heater temperature difference of 175 °C; values of 89 mW and 26 mW were obtained. Hence, roughly 63 mW is lost to topside convection and conduction through the gap. For an air conductivity of $2.6{\cdot}10^{-4}$ $W{\cdot}(cm{\cdot}°C)^{-1}$ and a 400 μm gap, about 7 mW is lost. The remaining 56 mW is given up to convection, and implies a coefficient *not greater than* $\sim 5{\cdot}10^{-2}$ $W{\cdot}(cm^2{\cdot}°C)^{-1}$. The value $h_{cv} = 3.5{\cdot}10^{-3}$ $W{\cdot}(cm^2{\cdot}°C)^{-1}$ slightly exceeds bulk values, but is less than the experimentally determined upper bound by an order of magnitude.

The predicted thermal conductivity of low-stress silicon nitride was $6.4{\cdot}10^{-2}$ $W{\cdot}(cm{\cdot}°C)^{-1}$, a value twice as large as those typically stated for SiN. This may be explained by chemical ordering maintained by Si-rich alloys and Si-Si bonds in the LPCVD silicon-rich films used here [11].

The TAS model, once proven on the case described here, was shown to have general applicability by comparisons with IR measurements made under a variety of conditions. Both square and circular membranes were simulated, and boundary conditions and drive voltages were manipulated. It is interesting to note that reducing the drive voltage from 4.48 V to 3.11 V required a reduction in the convection coefficient to $3.0{\cdot}10^{-3}$ $W{\cdot}(cm^2{\cdot}°C)^{-1}$. This is expected, since with decreasing temperature, buoyancy-induced convective currents are diminished.

CONCLUSIONS

It has been demonstrated that the TAS software can be used to accurately simulate the steady state and transient response of a microhotplate. With a minor modification to the existing design, adding an aluminum diffuser, the microhotplate adequately meets all the requirements for the preconcentration stage of Sandia's μChemLab project. Future modeling efforts will be directed at improving the heater design.

ACKNOWLEDGEMENTS

The authors would like to thank J.J. Mulhall and R. Mitchell for their assistance with IR temperature measurements. Sandia is a multiprogram laboratory operated by Sandia Corporation, a Lockheed Martin Company, for the United States Department of Energy under contract DE-AC04-94AL85000.

REFERENCES

[1] G.C. Frye-Mason, et. al., μ-TAS '98, Banff, Canada, October 12-16, 1998.

[2] N.R. Swart, and A. Nathan, *Sensors and Actuators A*, 43 (1994) 3-10.

[3] C.H. Mastrangelo, "Thermal Applications of Microbridges," Ph.D. Dissertation, U.C. Berkeley, 1991.

[4] E.D. Pallik, "Handbook of Optical Constants of Solids," Vols. I-II, Academic Press, 1985.

[5] T. Sato, *Japan. Journal of Phys.*, 6 (1967) 339-347.

[6] H.O. McMahon, *Journal of The Optical Society of America*, 40 (1950) 376-380.

[7] CRC Handbook of Chemistry and Physics, 1990.

[8] R.P. Manginell, J.H. Smith and A.J. Ricco, *Smart Structures and Materials*, SPIE Vol. 3046 (1997) 273-284.

[9] Y.S. Touloukian, R.W. Powell, C.Y. Ho, P.G. Klemens, "Thermophysical Properties of Matter" Vol. 4, Plenum, 1970.

[10] F. Kreith, "Principles of Heat Transfer," International Textbook Company, Scranton, PA, 1968.

[11] S. Habermehl, *J. Appl. Phys.*, 83 (1998) 4672.